

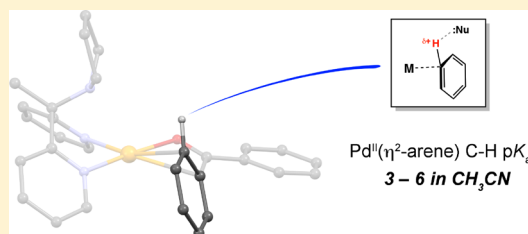
Absolute Estimates of Pd^{II}(η^2 -Arene) C–H Acidity

William E. Christman,^{ID} Travis J. Morrow, Navamoney Arulsamy,^{ID} and Elliott B. Hulley*^{ID}

Department of Chemistry, University of Wyoming, Laramie, Wyoming 82071, United States

S Supporting Information

ABSTRACT: Thermodynamic acidity is one of the most widely used quantities for characterizing proton transfer reactions. Measurement of these values for catalytically relevant species can be challenging, often requiring direct observation of equilibria. The C–H bonds of aromatic substrates are proposed to become substantially polarized during electrophilic activation, but quantifying the absolute acidity of the intermediate $M(\eta^2\text{-arene})$ complexes is highly challenging. Using a system that intercepts nascent protons at electrophilic Pd^{II} arene complexes, a combined experimental and computational study has demonstrated these C–H bonds to be far more acidic ($\text{p}K_{\text{a}}^{\text{CH}_3\text{CN}} = 3\text{--}6$) than many “nonbasic” substrates and additives that are present in electrophilic C–H activation catalysis, and the catalytic roles of these species may need to be reassessed.



INTRODUCTION

Nonpolar C–H bonds are notoriously difficult to break, often requiring preactivation prior to cleavage. Although a vast array of synthetic tactics have been developed, many strategies involve electrophilic activation.^{1–6} Aromatic substrates are particularly susceptible to this form of attack due to the interaction between π -electrons and electrophilic metal centers. Substrate coordination to electrophiles increases acidity by many orders of magnitude,^{7,8} and determining the degree of substrate acidification is important for understanding and predicting the course of protogenic reactions.

Electrophilic activation pathways are essential to Electrophilic Aromatic Substitution ($S_{\text{E}}\text{Ar}$)^{9,10} and Concerted Metalation Deprotonation (CMD)^{11–13} mechanisms in late-metal C–H functionalization.^{2,14} Bonding between aromatic π -orbitals and metals is electronically flexible, and the two-electron M –arene interactions relevant to M – C_{aryl} bond formation can be described on a continuum between η^2 -arene and η^1 -arenium extremes (Figure 1).^{15,16} These intermediates

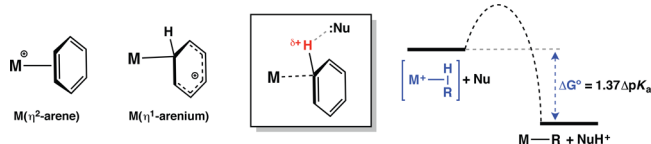


Figure 1. In base-mediated arene activation, η^2 -coordination activates C–H bonds toward deprotonation via exogenous bases.

are implicated in electrophilic activation of aromatic molecules, wherein nucleophiles deprotonate the acidified C–H bond with concomitant metalation. The driving force for this metalation, which is ultimately a proton transfer reaction, can be expressed as a difference in acidity ($\Delta\text{p}K_{\text{a}}$) between the η^2 -arene complex and protonated base product (Figure 1, right).

For a given nucleophile, $\Delta\text{p}K_{\text{a}}$ is also a direct reflection of the acidification of the substrate C–H bond. Characterizing and tracking these acidity changes is essential to energy-matching of reaction intermediates.^{17,18} Despite the obvious importance to late-metal arylation chemistry, it is usually impossible to directly measure the relevant equilibria to determine the extent of substrate acidification. The intrinsically high reactivity of late-metal arene complexes and competitive binding of exogenous nucleophiles (e.g., solvents and Brønsted bases) usually render the π -bound intermediates unobservable. Catalytic systems often rely on small, anionic, terminal bases (e.g., CO_3^{2-} , CH_3CO_2^-) and weakly polar solvents (e.g., THF, toluene), both of which complicate the calculation of relative acidities of relevant intermediates. Thus, although the energetics of proton transfers (ΔG° and ΔG^\ddagger) can be readily calculated to evaluate competing mechanisms, relating those values back to thermodynamic acidities requires accurately calculating the standard states of base and conjugate acid and using a solvent with an absolute $\text{p}K_{\text{a}}$ scale (e.g., relative to protonated solvent). Circumventing these limitations is critical to determining the $\text{p}K_{\text{a}}$ of metal-bound arene C–H bonds.

One strategy for avoiding the aforementioned complications is to employ a pendant-base ligand that is capable of intercepting the C–H activation product prior to intermolecular proton loss without hindering the formation of the η^2 -arene intermediate. The present work reports efforts to study Pd-mediated C–H activation using this approach, wherein a basic pyrrolidine moiety is tethered to an electrophilic Pd^{II} complex bearing highly labile ancillary ligands.

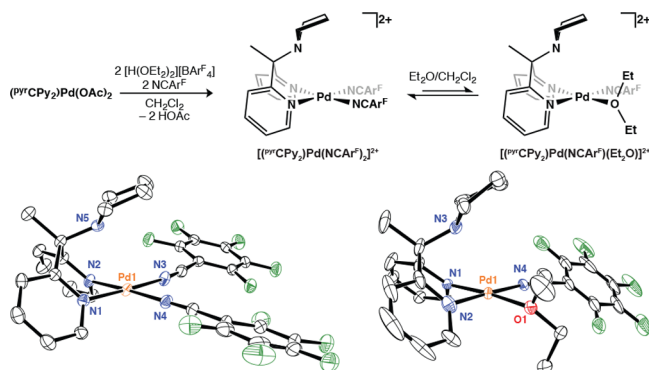
RESULTS AND DISCUSSION

Addition of 2,2'-(1-(pyrrolidin-1-yl)ethane-1,1-diyl)dipyridine (PyrCPy_2)¹⁹ to a dichloromethane suspension of $\text{Pd}(\text{OAc})_2$

Received: May 23, 2018

leads to precursor $(\text{Pyr}^{\text{H}}\text{CPy}_2)\text{Pd}(\text{OAc})_2$, which releases HOAc upon treatment with 2 equiv of the strong acid $[\text{H}(\text{OEt}_2)_2][\text{BAR}^{\text{F}}_4]$ ($\text{Ar}^{\text{F}} = \text{C}_6\text{F}_5$) in the presence of excess pentafluorobenzonitrile (NCAr^{F}) to yield purple $[(\text{Pyr}^{\text{H}}\text{CPy}_2)\text{Pd}(\text{NCAr}^{\text{F}})_2][\text{BAR}^{\text{F}}_4]_2$ (Scheme 1). When recrystallized from a

Scheme 1. Synthesis and Solid State Structures of the $\text{BAR}^{\text{F}}_4^-$ Salts of $[(\text{Pyr}^{\text{H}}\text{CPy}_2)\text{Pd}(\text{NCAr}^{\text{F}})_2]^{2+}$ and $[(\text{Pyr}^{\text{H}}\text{CPy}_2)\text{Pd}(\text{NCAr}^{\text{F}})(\text{OEt}_2)]^{2+}$ ($\text{Ar}^{\text{F}} = \text{C}_6\text{F}_5$) Plotted with 30% Probability Ellipsoids

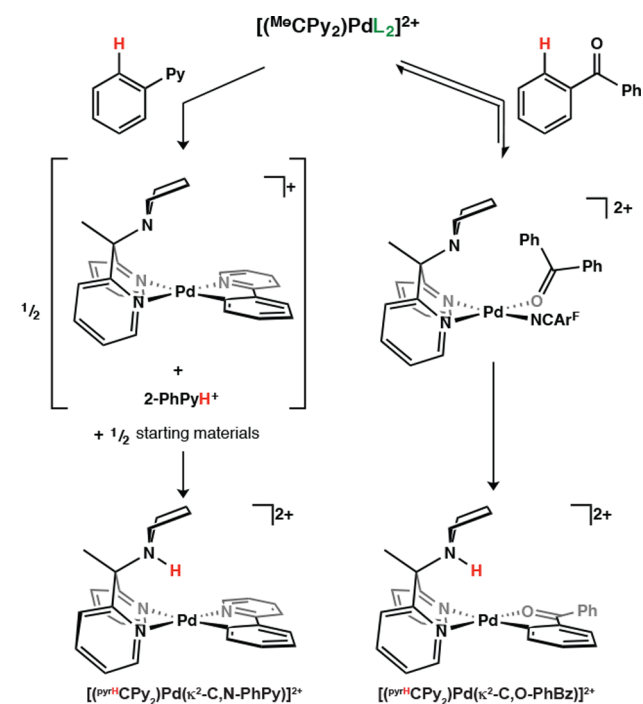


1:1 solution of $\text{CH}_2\text{Cl}_2/\text{Et}_2\text{O}$, the ether adduct $[(\text{Pyr}^{\text{H}}\text{CPy}_2)\text{Pd}(\text{NCAr}^{\text{F}})(\text{OEt}_2)][\text{BAR}^{\text{F}}_4]_2$ can be isolated as red crystals. Both complexes are active for aryl C–H activation, with the ether adduct being more useful for kinetic studies with weakly binding substrates.

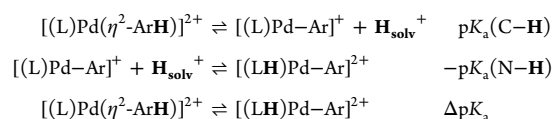
Although stable in CH_2Cl_2 solution for days at elevated temperatures ($\sim 50^\circ\text{C}$, sealed tube), $[(\text{Pyr}^{\text{H}}\text{CPy}_2)\text{Pd}(\text{NCAr}^{\text{F}})_2]^{2+}$ is highly reactive with aryl C–H bonds in substrates bearing directing groups. When treated with 2-phenylpyridine (2-PhPy) or benzophenone (Ph_2CO), formation of N-protonated (pyrrolidinium) cyclometalated products occurs readily at low temperature ($< 0^\circ\text{C}$, Scheme 2), although the kinetics are complicated by competing equilibria. For example, the orthometallation of 2-PhPy appears to be mediated by the substrate itself, forming the cyclometallate monocation as the kinetic product alongside half an equivalent of 2-PhPyH⁺ ($\text{p}K_{\text{a}}(\text{NH}) = 11.9$ in CH_3CN).^{20,21} Although 2-PhPy is evidently more basic than the pendant pyrrolidinium (see below), protonation equilibria must regenerate free 2-PhPy and allow formation of the N-protonated cyclometallate $[(\text{Pyr}^{\text{H}}\text{CPy}_2)\text{Pd}(\kappa^2\text{-C,N-PhPy})]^{2+}$ as the thermodynamic product. Orthometallation of benzophenone is also facile, although considerably slower due to competitive binding of NCAr^{F} relative to the benzophenone oxygen, and both electrophilic Pd complexes exhibit complex reaction kinetics that are still under study. The free-base cyclometallate monocations $[(\text{Pyr}^{\text{H}}\text{CPy}_2)\text{Pd}(\kappa^2\text{-C,N-PhPy})]^+$ and $[(\text{Pyr}^{\text{H}}\text{CPy}_2)\text{Pd}(\kappa^2\text{-C,O-PhBz})]^+$ are readily prepared from addition of K_2CO_3 , and can be cleanly reprotonated with $[\text{H}(\text{OEt}_2)_2][\text{BAR}^{\text{F}}_4]$. The protonated and unprotonated species can all be isolated in crystalline form; the solid-state structures of $[(\text{Pyr}^{\text{H}}\text{CPy}_2)\text{Pd}(\kappa^2\text{-C,O-PhBz})]^+$ and $[(\text{Pyr}^{\text{H}}\text{CPy}_2)\text{Pd}(\kappa^2\text{-C,O-PhBz})]^{2+}$ are shown in Figure 2.

The driving force for any proton transfer reaction can be expressed as the difference of the acidities of each protonated species (i.e., $\Delta G^\circ = 1.37\Delta\text{p}K_{\text{a}}$). Accordingly, since the intermediate η^2 -arene complexes are clearly less stable than the N-protonated cyclometallates, the pendant pyrrolidinium must be less acidic than the C–H bond of the η^2 -arene.

Scheme 2. Binding and Cyclometallation of 2-Phenylpyridine (Left) and Benzophenone (Right) at $[(\text{Pyr}^{\text{H}}\text{CPy}_2)\text{PdL}_2]^{2+}$ ($\text{L}_2 = (\text{NCAr}^{\text{F}})_2$ and $(\text{NCAr}^{\text{F}})(\text{Et}_2\text{O})$)



Determining the absolute acidity of the target Pd-bound C–H bond requires (1) an anchor complex that is stable in the solvent of choice (i.e., the N-protonated cyclometallate) and (2) knowledge of the free energy difference (via $\Delta\text{p}K_{\text{a}}$) between the target and the anchor complex (i.e., the driving force of cyclometallation and proton transfer, $\Delta G_{\text{cyclomet}}$):



Acid–base equilibria between $[(\text{Pyr}^{\text{H}}\text{CPy}_2)\text{Pd}(\kappa^2\text{-C,N-PhPy})]^+$ and two reference acids ($\text{BAR}^{\text{F}}_4^-$ salts of 2-methylanilinium and *N,N*-dimethylanilinium) were measured in acetonitrile, yielding a $\text{p}K_{\text{a}}$ of 11.1(1) for the pendant pyrrolidinium in the 2-PhPy cyclometallate (details in the Supporting Information). The pyrrolidine moiety in the dicationic complex is considerably less basic than the parent base *N*-methylpyrrolidine ($\text{p}K_{\text{a}}(\text{NH}) = 18.42$ in CH_3CN),²² a fact that is consistent with known correlations between acidity and charge.²³

This complex is our experimental reference point for other complexes in the study; displacement of the labile ketone by CH_3CN thwarted attempts to directly measure the basicity of the pyrrolidine in $[(\text{Pyr}^{\text{H}}\text{CPy}_2)\text{Pd}(\kappa^2\text{-C,O-PhBz})]^+$. Although both the protonated and unprotonated forms are stable on their own in CH_2Cl_2 , $[(\text{Pyr}^{\text{H}}\text{CPy}_2)\text{Pd}(\kappa^2\text{-C,O-PhBz})]^+$ reversibly reacts with anilines to form an as-yet unidentified product and thus cannot be directly subjected to $\text{p}K_{\text{a}}$ measurements. The pendant pyrrolidine readily exchanges with $[(\text{Pyr}^{\text{H}}\text{CPy}_2)\text{Pd}(\kappa^2\text{-C,N-PhPy})]^{2+}$, however, and the $\Delta\text{p}K_{\text{a}}$ between these two N-protonated cyclometallates can be readily measured (0.1(1), where the $[(\text{Pyr}^{\text{H}}\text{CPy}_2)\text{Pd}(\kappa^2\text{-C,O-PhBz})]^{2+}$ is less acidic). Given the relatively minor differences between these

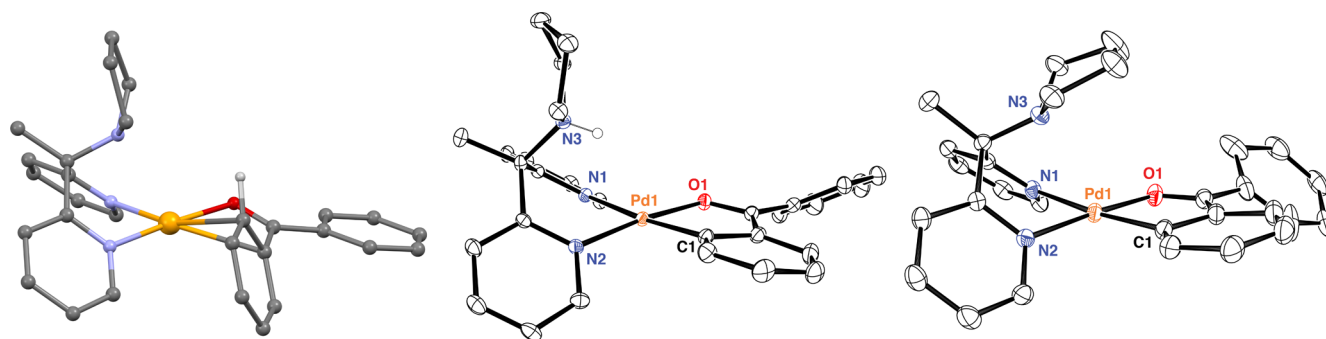


Figure 2. Calculated structure of $[(\text{pyr}^{\text{H}}\text{CPy}_2)\text{Pd}(\kappa^2, \eta^2\text{-Ph, C}=\text{CH-PhBz})]^{2+}$ (left) and the solid state structure of $[(\text{pyr}^{\text{H}}\text{CPy}_2)\text{Pd}(\kappa^2\text{-C, O-PhBz})]^{2+}$ (middle) and $[(\text{pyr}^{\text{H}}\text{CPy}_2)\text{Pd}(\kappa^2\text{-C, O-PhBz})]^{2+}$ (right) plotted with 30% probability ellipsoids. Anions (SbF_6^- or $\text{BAR}_4^{\text{F}}^-$) and hydrogen atoms (except for the *ortho*-C–H of the η^2 -arene complex and nascent N–H) have been omitted. See Table S3 for a list of relevant distances and angles.

pyrrolidines, the small difference in pK_a is unsurprising and likely to be conserved in CH_3CN .

The free energy for cyclometalation and proton transfer (ΔG_{cymet}) is less accessible with experimentation alone. Although such species are along the path from substrate to activation product²⁴ and related complexes have even been observed and crystallized on occasion,^{15,25–30} the $\text{Pd}(\eta^2\text{-arene})$ intermediates in the present report have not yet been directly observed. As discussed above, however, accurate free energies for intramolecular proton transfers are calculable via modern DFT methods. In the present case, since the process is formally unimolecular and there is no net change in complex charge, many of the potential issues with DFT studies are mitigated. The calculated structures for the N-protonated and non-protonated cyclometallates agree well with the solid-state structures, and the structural parameters for the $\text{Pd}(\eta^2\text{-arene})$ structures are consistent with related compounds from prior computational investigations and structures characterized in the solid state (see Supporting Information for more details).^{15,25} The ΔG_{cymet} for C–H activation of bound 2-phenylpyridine (Figure 3) is calculated to be -9.5 kcal/mol in

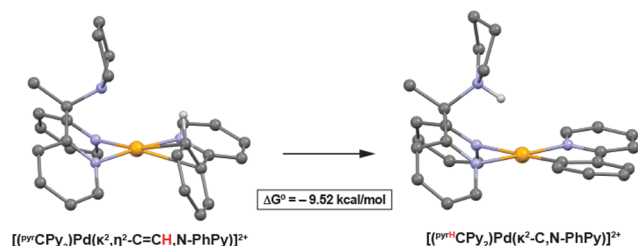


Figure 3. Calculated structures and relative energy ($\Delta G_{\text{cymet}}^\circ$ in CH_3CN solvent) of $[(\text{pyr}^{\text{H}}\text{CPy}_2)\text{Pd}(\kappa^2, \eta^2\text{-C}=\text{CH, N-PhPy})]^{2+}$ and $[(\text{pyr}^{\text{H}}\text{CPy}_2)\text{Pd}(\kappa^2\text{-C, N-PhPy})]^{2+}$. Computational details and structural parameters for all calculated species are available in the Supporting Information.

CH_3CN with the M06-2X functional,³¹ def2-basis sets (def2-QZVP for Pd and def2-TZVP for all other atoms),³² and a continuum-based solvation model (SMD).³³

A survey of functionals (M06-L, M06-2X, ωB97XD , and B3LYP) and solvation models (SMD and CPCM) revealed a relatively narrow range of values for $\Delta G_{\text{cymet}}^\circ$ for 2-PhPy (-7.2 to -11.4 kcal/mol, considering both CH_3CN and CH_2Cl_2); thus, the chosen benchmark value of -9.5 kcal/mol is likely to be a reasonable estimate of the real value.

Since both the protonated and unprotonated forms are stable in acetonitrile, the pK_a of the pyrrolidinium in $[(\text{pyr}^{\text{H}}\text{CPy}_2)\text{Pd}(\kappa^2\text{-C, N-PhPy})]^{2+}$ can be used as an anchor for other compounds. The pK_a of $[(\text{pyr}^{\text{H}}\text{CPy}_2)\text{Pd}(\kappa^2\text{-C, O-PhBz})]^{2+}$, for example, can be computationally derived from an isodesmic proton transfer and the pK_a of its η^2 -arene precursor determined from the DFT-derived ΔG_{cymet} . The combined results of the experimental and computational investigations are presented in Figure 4, where the pK_a values in CH_3CN are

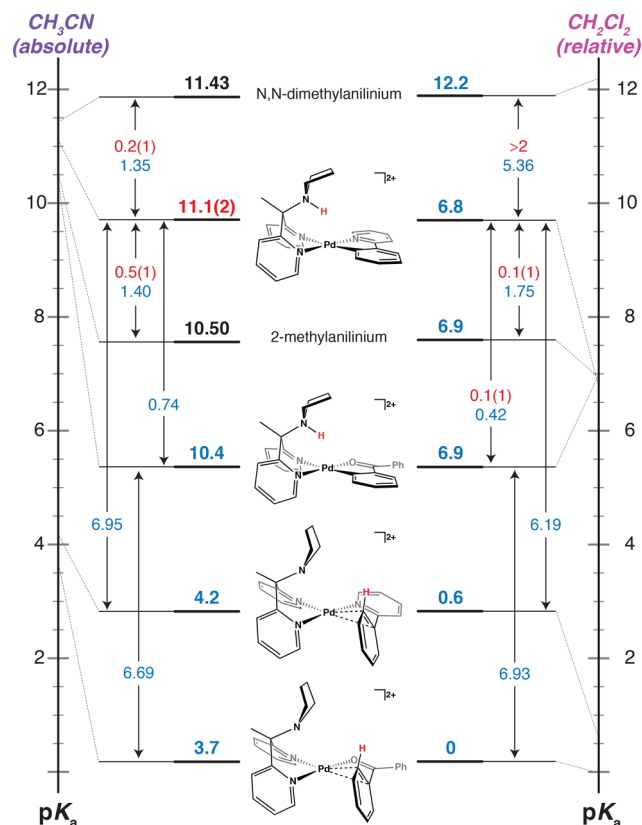


Figure 4. Graphical depiction of literature (black),³⁴ experimental (red), and calculated (blue) pK_a values in CH_3CN (as absolute values, relative to $[\text{CH}_3\text{CNH}]^+$) and CH_2Cl_2 (as relative values). The experimentally and computationally derived equilibria that lead to these pK_a values are shown on the arrows between relevant species. Note that the relative order of 2-methylaniline and the N-protonated Pd-cyclometallates of benzophenone and 2-phenylpyridine changes between solvents.

relative to those of CH_3CNH^+ and those in CH_2Cl_2 are relative to those of the most acidic compound in this study. In cases where experimental equilibria were measured within a given solvent, experimental $\Delta\text{p}K_a$ s were used instead of DFT-derived values.

On the basis of a brief comparison between experimental and DFT-derived $\text{p}K_a$'s, the calculated C–H acidities of the η^2 -arene complexes are likely to be overestimated by 1–2 $\text{p}K_a$ units. For example, the calculated $\Delta\text{p}K_a$ between reference anilinium acids in CH_3CN (2.8) is significantly larger than the experimental value (1.1), and is calculated to be larger still in CH_2Cl_2 (3.6). This difference is significantly larger than expected on the basis of known aniline basicity trends in dichloroethane (which should be similar to dichloromethane)³⁵ and may be a result of ignoring discrete solvation or ion-pairing effects. Nonetheless, the calculated $\Delta\text{p}K_a$ between the two N-protonated cyclometallates in CH_2Cl_2 (0.4) is much closer to the experimental value (0.1(1)) than those calculated between Pd species and anilines and suggests those values are more accurate. For these reasons, the calculated C–H acidities reported here are assumed to be upper estimates (i.e., the real $\text{p}K_a$ values are somewhat higher than computed by DFT).

The modest energy difference between the η^2 -arenes and their cyclometalated products suggested that protolytic arene exchange would be kinetically observable. Since C–H activation of Ph_2CO by $[(\text{pyr}^{\text{H}}\text{CPy}_2)\text{Pd}(\text{NCAr}^{\text{F}})_2]^{2+}$ is fast above 20 °C, kinetic limitations of protolytic aryl exchange would be largely due to the energetic cost of accessing the η^2 -arene intermediate (i.e., $\Delta G_{\text{cymet}}^\circ$). Indeed, heating a CD_2Cl_2 solution of $[(\text{pyr}^{\text{H}}\text{CPy}_2)\text{Pd}(\kappa^2\text{-C,O-PhBz})]^{2+}$ with 20 equiv of benzophenone-*d*₁₀ in a sealed NMR tube led to ~90% conversion to $[(\text{pyr}^{\text{D}}\text{CPy}_2)\text{Pd}(\kappa^2\text{-C,O-PhBz-}d_9)]^{2+}$ within 8 days at 60 °C. Studies are ongoing with ligand frameworks bearing weaker pendant bases to examine the kinetic and thermodynamic landscape of protolytic arene exchange.

The high acidity of $\text{Pd}^{\text{II}}(\eta^2\text{-arene})$ C–H bonds (e.g., $\text{p}K_a^{\text{CH}_3\text{CN}}$ of 3–6 in the present study) implies that polar solvents, ancillary additives, byproducts and impurities may play important roles in Pd-catalyzed electrophilic C–H activation. Even deprotonation reactions that are formally unfavorable (negative $\Delta\text{p}K_a$) may be mechanistically relevant, as a $\Delta\text{p}K_a$ of –2 would correspond to a free energy cost of only ~3 kcal/mol (under standard conditions). Indeed, the $\text{p}K_a$ values (CH_3CN) for the conjugate acids of water ($\text{p}K_a[\text{H}_3\text{O}^+] = 2.15$),³⁶ “spectator” anions ($\text{p}K_a[\text{HOTf}] = 2.60$, $\text{p}K_a[\text{HCl}] = 8.94$),^{37,38} N- and P-based ligands ($\text{p}K_a[\text{HNR}_3] = 1\text{--}19$, $\text{p}K_a[\text{HPR}_3] = 4\text{--}16$),³⁹ and common organic functional groups (e.g., amides, $\text{p}K_a[\text{N}=\text{COH}^+] = 5\text{--}7$)⁴⁰ are such that these moieties may be kinetically competent for deprotonation of acidic C–H bonds. Additionally, many potential bases are subject to homoconjugation equilibria that increase their apparent basicity (e.g., $\text{p}K_a[\text{H}(\text{MeOH})_2^+] = 3.1$, $\text{p}K_a[\text{H}(\text{H}_2\text{O})_3^+] = 4.52$, $\text{p}K_a[\text{Cl-H-Cl}^-] = 11.17$);^{36,37} thus, the deprotonation potential of many substrates and/or additives may have a significant concentration dependence.

Solvation is of critical importance when evaluating absolute and relative acidities. Polar solvents will stabilize charged species more than nonpolar solvents, but polar solvents can also mitigate acidity differences (e.g., $\Delta\text{p}K_a$) more than nonpolar solvents,⁴¹ such that there can be considerable variation in the relative $\text{p}K_a$ values of acids in different solvents. For example, although the $\text{p}K_a$ of methanol in CH_3CN (as the

homoconjugate $\text{H}(\text{CH}_3\text{OH})_2^+$) is only 3.1; addition of ~30 equiv of methanol to yellow $[(\text{pyr}^{\text{H}}\text{CPy}_2)\text{Pd}(\kappa^2\text{-C,O-PhBz})]^{2+}$ in CH_2Cl_2 results in complete deprotonation and formation of red $[(\text{pyr}^{\text{H}}\text{CPy}_2)\text{Pd}(\kappa^2\text{-C,O-PhBz})]^+$. Conversely, addition of 1 equiv of crystalline $[\text{H}(\text{CH}_3\text{OH})_{1.5}]^+[\text{BAR}^{\text{F}}_4]^-$ to solutions of $[(\text{pyr}^{\text{H}}\text{CPy}_2)\text{Pd}(\kappa^2\text{-C,O-PhBz})]^+$ results in complete pyrrolidine protonation. Thus, protonated methanol (likely as the homoconjugate $\text{H}(\text{CH}_3\text{OH})_2^+$) is only slightly less acidic than the pyrrolidinium proton in $[(\text{pyr}^{\text{H}}\text{CPy}_2)\text{Pd}(\kappa^2\text{-C,O-PhBz})]^{2+}$ in CH_2Cl_2 (e.g., $\Delta\text{p}K_a \sim 1\text{--}2$). Since the corresponding η^2 -arene intermediate is more acidic, C–H deprotonation by methanol would be favorable by ~5–7 kcal/mol.

These results quantify the substantial increase in the acidity of arene C–H bonds upon coordination. Although absolute $\text{p}K_a$ values for arenes are essentially impossible to measure directly (since they require the formation of free aryl anions in solution), the $\text{p}K_a$ of benzene can be estimated by a series of thermochemical cycles to be 48 in CH_3CN .^{42–45} Thus, as is observed with H_2 coordination to electrophilic metals,⁴⁶ coordination of arenes to Pd^{II} can increase the acidity of C–H bonds by ≥ 40 orders of magnitude.

CONCLUSIONS

Many of the computational investigations of related catalytic systems have focused on intramolecular C–H activation by basic additives already bound to Pd.⁴⁷ The present report highlights the potential mechanistic importance of intermolecular activations, given that many additives are basic enough to participate. Water contamination may be especially important,⁴⁸ as water molecules are kinetically adept at relaying protons from acidified substrates.^{49–52} The C–H $\text{p}K_a$'s presented here may even be an upper estimate on what may be operative in some systems (e.g., those using Ag^+ additives), given the potential for Ag^+ to increase apparent electrophilicity by forming Pd–Ag bimetallics or facilitating access to Pd(III) species.^{53–55} Studies are ongoing to determine the kinetic role (if any) of the pendant amine, weakly basic substrates (e.g., Ph_2CO), and inadvertent solvents (e.g., Et_2O) in the C–H activation of η^2 -arene intermediates. These experiments are part of a longer-term effort to use $\text{p}K_a$ and ligand-binding equilibria to determine heterolytic M–C bond dissociation energies ($\Delta G_{\text{R-}}$).

EXPERIMENTAL SECTION

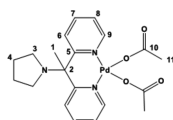
General. All operations were performed at an altitude of 7220 ft (ambient pressure 0.77 atm); a list of pressure-corrected boiling points for the solvents used in this report can be found in the [Supporting Information](#). Unless otherwise noted, solvents used in syntheses were purified by passing through the neutral alumina columns of an Innovative Technology, Inc., Pure Solv purification system, followed by degassing and storage in a glovebox over activated 3 Å molecular sieves. Elemental analyses were performed by Atlantic Microlab in Norcross, GA. Syntheses reported to occur at “ambient temperature” should be taken as 22 ± 3 °C. The compounds 1-pyrrolidinyl-1,1-(2,2-dipyridyl)ethane ($\text{pyr}^{\text{H}}\text{CPy}_2$) and $[\text{H}(\text{OEt}_2)_2][\text{B}(\text{C}_6\text{F}_5)_4]$ (from $\text{KB}(\text{C}_6\text{F}_5)_4$, purchased from Boulder Scientific) were prepared according to published procedures.^{19,56} Synthetic details and characterization data for the BAR^{F}_4 salts of 2-methylanilinium, 2,6-diisopropylanilinium, and *N,N*-dimethylanilinium are available in the [Supporting Information](#). All other starting materials were purchased from Strem or Sigma-Aldrich and used as received.

NMR Spectroscopy. All operations utilized resealable NMR tubes (J. Young). Unless otherwise noted, NMR experiments were taken at

26.5 ± 1 °C. Temperatures quoted for NMR experiments are based on calibrations and have an uncertainty of ±0.5 °C. NMR spectra were obtained on a BRUKER 400 spectrometer. NMR chemical shifts are reported relative to deuterated solvent signals (for ¹³C NMR) or residual protio solvent signals (for ¹H NMR).⁵⁷ Deuterated solvent signals and residual protio solvent signals are designated by (*) in the reported NMR spectra. Deuterated NMR solvents were purchased from Cambridge Isotopes Laboratories, dried over 3 Å molecular sieves under N₂ and then vacuum distilled. The ¹³C resonances of the B(C₆F₅)₄⁻ anion are typically broad (from ¹⁹F coupling and ¹⁰B/¹¹B quadrupolar broadening) and have been omitted from tabulated NMR spectral data in cases where they are not clearly distinguishable. From the ¹³C NMR spectrum of *N,N*-dimethylanilinium B(C₆F₅)₄⁻ in CD₂Cl₂ we were able to clearly identify the *ortho* (148.57, d, *J* = 241 Hz), *meta* (136.84, d, *J* = 243 Hz), *para* (138.68, d, *J* = 248 Hz), and *ipso* (124.30, m) resonances. Instead, the ¹⁹F spectra are reported that clearly show the presence of the B(C₆F₄)₄⁻ anion. The assignments of NMR resonances are listed in reference to chemical structures shown below each synthetic description.

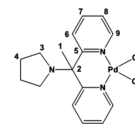
Computational Methods. Calculations were performed with the Gaussian09 software package.⁵⁸ The M06-2X,³¹ M06-L,⁵⁹ ωB97XD,⁶⁰ and B3LYP⁶¹ functionals were evaluated in conjunction with the def2 basis sets from the Alrichs group (def2-TZVPD basis set for H/C/N/O atoms and def2-QZVPD (with effective core potentials) for Pd).⁶² The B3LYP functional was also used in conjunction with the SDD basis set during initial computational investigations.⁵⁹ The CPCM and SMD solvation models were used with both CH₂Cl₂ and CH₃CN as solvents.^{32,59,63} Frequency calculations were performed on all minimized structures to confirm the absence of imaginary frequencies.

(^{Py}CPy₂)Pd(OAc)₂ (2). 2,2'-(1-(Pyrrolidin-1-yl)ethane-1,1-diyl)-dipyridine (^{Py}CPy₂, 1.10 g, 4.34 mmol, 1.0 equiv) was added to a 250 mL Schlenk flask with a stir bar and ~100 mL of dichloromethane. Palladium(II) acetate (0.975 g, 4.34 mmol, 1.0 equiv) was added to the flask, and the solution was left to stir for 18 h during which time the solution turns golden in color. The solvent was removed *in vacuo*, and the resulting light brown powder was washed over a glass filter frit with diethyl ether (to remove a bright yellow impurity) followed by a washing with hexane. The resulting light brown powder was dried under reduced pressure (2.03 g, 98%). ¹H NMR (400 MHz, CD₂Cl₂): δ 8.54 (d, *J*_{HH} = 4 Hz, 2H, H9), 7.87 (t, *J*_{HH} = 8 Hz, 2H, H7), 7.73 (br. s, 2H, H6), 7.35 (t, *J*_{HH} = 6 Hz, 2H, H8), 3.00 (br. s, 4H, H3), 2.47 (s, 3H, H1), 1.90 (s, 6H, H11), 1.83 (br. s, 4H, H4). ¹³C{¹H} NMR (151 MHz, CD₂Cl₂): δ 177.45 (C10), 150.44 (C9), 138.65 (C7), 124.81 (C6), 124.48 (C8), 78.11 (C2), 24.51 (C4), 23.49 (C11). C3 was buried under the solvent peak, and C1 and C5 are not visible due to exchange broadening. 2 was not found to be analytically pure by elemental analysis, but impurities apparently do not hinder subsequent reactions. The structure of the diacetate is shown below as a guide to assigning protons only; obviously the structure of Pd(acetate) compounds varies considerably.^{13,64}

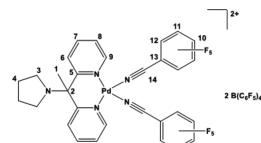


(^{Py}CPy₂)PdCl₂ (3). 2,2'-(1-(Pyrrolidin-1-yl)ethane-1,1-diyl)-dipyridine (^{Py}CPy₂, 545 mg, 2.15 mmol, 1.0 equiv) was added to a 100 mL Schlenk flask with a stir bar and ~50 mL of dichloromethane. Dichlorobis(acetonitrile)Pd(II) (558 mg, 2.15 mmol, 1.0 equiv) was then added while the solution was stirring. The initial gold color of the solution gradually changed to a dark reddish/brown over an hour. The solution was left to stir overnight, and the next day the solvent was removed *in vacuo* to give a tan powder that was washed with hexane over a filter frit. The product was dried under reduced pressure (880 mg, 95%). 3 can be recrystallized with difficulty to give brown needlelike crystals from a sealed solution of dichloromethane layered with an equal amount of hexane left at room temperature for 3 days. Yields of the recrystallized product are <10%. ¹H NMR (400 MHz, CD₂Cl₂): δ 9.10 (d, *J*_{HH} = 5 Hz, 2H, H9), 7.86 (t, *J*_{HH} = 8 Hz, 2H, H7), 7.54 (d, *J*_{HH} = 8 Hz, 2H, H6), 7.33 (t, *J*_{HH} = 7 Hz, 2H, H8),

2.79 (br. s, 2H, H3), 2.57 (br. s, 2H, H3), 2.28 (br. s, 2H, H4), 2.14 (s, 3H, H1), 1.77 (br. s, 2H, H4). ¹³C{¹H} NMR (151 MHz, CD₂Cl₂): δ 159.22 (C5), 154.34 (C9), 139.42 (C7), 124.52 (C8), 123.04 (C6), 47.91 (C3), 24.72 (C4). C1 and C2 are not observable due to exchange broadening. Before EA, 3 was placed under high vacuum for 72 h and afterward was found to contain 0.3 equiv of dichloromethane by ¹H NMR. Anal. Calcd for C₁₆H₁₉Cl₂N₃Pd·0.3 CH₂Cl₂: C, 42.92; H, 4.33; N, 9.21. Found: C, 42.92; H, 4.41; N, 9.01.

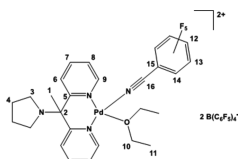


[(^{Py}CPy₂)Pd(NCAr^F)₂]²⁺[BAR^F₄]⁻² (4). Compound 2 (278 mg, 0.58 mmol, 1.0 equiv) was added along with NCAr^F (Ar^F = C₆F₅CN, 0.25 mL, 2.00 mmol, 3.4 equiv) to a 100 mL Schlenk flask with a stir bar and 30 mL of dichloromethane. With the solution stirring vigorously, [H(OEt₂)₂]⁺[BAR^F₄]⁻ (964 mg, 1.16 mmol, 2.0 equiv) was added slowly over the course of 3 min. The solution was a deep red color after the addition of the acid. The reaction mixture was allowed to stir for 30 min before the solvent was removed *in vacuo*. A 10 mL aliquot of hexane was added to the purple residue and subsequently decanted to remove any leftover acetic acid. This was repeated one more time. The residue was recrystallized from ~15 mL of dichloromethane layered with ~15 mL of hexane left overnight at room temperature in a sealed Schlenk flask (805 mg, 66%). 4 exhibits low solubility in most solvents including dichloromethane. 4 can be placed in a sonication bath to temporarily increase solubility although it will recrystallize from solution over 24 h. ¹H NMR (400 MHz, CD₂Cl₂): δ 8.62 (d, *J*_{HH} = 5 Hz, 2H, H9), 8.18 (t, *J*_{HH} = 8 Hz, 2H, H7), 7.82 (d, *J*_{HH} = 8 Hz, 2H, H6), 7.56 (t, *J*_{HH} = 7 Hz, 2H, H8), 2.76 (s, 4H, H3), 2.21 (s, 3H, H1), 2.12 (s, 4H, H4). ¹³C{¹H} NMR (CD₂Cl₂): δ 158.09 (C5), 152.57 (C9), 149.51, (d, *J*_{CF} = 273 Hz, C12), 148.44 (d, *J*_{CF} = 241 Hz, *o*-B(C₆F₅)₄), 143.97 (C8), 138.70 (d, *J*_{CF} = 257 Hz, *p*-B(C₆F₅)₄), 136.67 (*J*_{CF} = 246 Hz, *m*-B(C₆F₅)₄), 127.48 (C7), 125.79 (C6), 113.89 (C14), 74.34 (C2), 50.04 (C3), 24.61 (C4), 12.09 (C1). C10, C11, and C13 are not clearly distinguishable from the baseline/other ¹³C peaks. ¹⁹F NMR (376 MHz, CD₂Cl₂): δ -127.55 (t, *J*_{FF} = 12 Hz, 4F, F12), -129.71 (m, 2F, F10), -133.30 (br. s, *ν*_{1/2} = 40 Hz, 16F, *o*-C₆F₅), -153.69 (t, *J*_{FF} = 18 Hz, 4F, F11), -163.39 (t, *J*_{FF} = 20 Hz, 8F, *p*-C₆F₅), -167.43 (t, *J*_{FF} = 17 Hz, 16F, *m*-C₆F₅). Anal. Calcd for C₇₈H₁₉B₂F₅₀N₅Pd: C, 44.53; H, 0.91; N, 3.33. Found: C, 44.80; H, 0.85; N, 3.38.

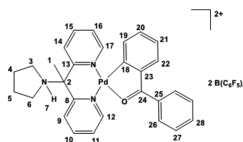


[(^{Py}CPy₂)Pd(OEt₂)(NCAr^F)]²⁺[BAR^F₄]⁻² (5). Compound 4 (172 mg, 0.087 mmol, 1.0 equiv) was dissolved in 15 mL of 50/50 diethyl ether/dichloromethane solution in a sealed 20 mL scintillation vial. The solution was left overnight at room temperature and pale red plate-like crystals formed by morning (78 mg, 48%). The crystals of 5 may need to be recrystallized one to two more subsequent times to improve purity. This compound slowly decomposes if left in solution at room temperature. Yield: 78 mg, 48%. ¹H NMR (400 MHz, CD₂Cl₂): δ 8.51 (br. s, 2H, H9), 8.11 (t, *J*_{HH} = 8 Hz, 2H, H7), 7.66 (d, *J*_{HH} = 8 Hz, 2H, H6), 7.58 (t, *J*_{HH} = 7 Hz, 2H, H7), 4.09 (q, *J*_{HH} = 7 Hz, 4H, H10), 3.26 (br. s, 2H, H3), 2.73 (br. s, 2H, H3), 2.18 (multiple peaks, 7H, H4 and H1), 1.76 (t, *J*_{HH} = 7 Hz, 6H, H11). Free diethyl ether is observed at 3.45 and 1.15 in the ¹H NMR spectrum. ¹³C{¹H} NMR (101 MHz, CD₂Cl₂): δ 158.10 (C5), 149.33 (C9), 148.51 (d, *J*_{CF} = 240 Hz, *o*-B(C₆F₅)₄), 142.90 (C7), 138.60 (d, *J*_{CF} = 245 Hz, *p*-B(C₆F₅)₄), 136.68 (d, *J*_{CF} = 249 Hz, *m*-B(C₆F₅)₄), 127.05 (C8), 124.45 (C6), 82.55 (C2), 75.74 (C10), 58.22 (C3), 25.34 (C4), 15.80 (C1), 15.42 (C11). C12–C16 are not clearly distinguishable from the baseline/other ¹³C peaks. ¹⁹F NMR (376

MHz, CD₂Cl₂): δ -127.68 (t, $J_{\text{FF}} = 12$ Hz, 2F, F14), -128.97 (m, 1F, F12), -133.18 (br. s, $\nu_{1/2} = 40$ Hz, 16F, *o*-C₆F₅), -153.24 (t, $J_{\text{FF}} = 18$ Hz, 4F, F13), -163.46 (t, $J_{\text{FF}} = 20$ Hz, 8F, *p*-C₆F₅), -167.48 (t, $J_{\text{FF}} = 17$ Hz, 16F, *m*-C₆F₅). The majority of peaks visible in the NMR spectra that are not from **5** are from **4**. Anal. Calcd for C₇₅H₂₉B₂F₄₅N₄OPd: C, 45.38; H, 1.47; N, 2.82. Found: C, 45.39; H, 1.72; N, 2.88.

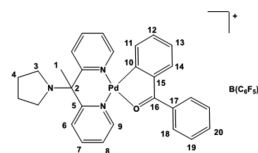


[(Pyr^HCPy₂)Pd(C₆H₄(OCC₆H₅))] ²⁺[BAR^F₄⁻]₂ (6**). Compound **4** (161 mg, 0.077 mmol, 1.0 equiv) was added to a 20 mL scintillation vial with a stir bar and 10 mL of dichloromethane. Benzophenone (139 mg, 0.77 mmol, 10 equiv) was added, and the solution was allowed to stir for 6 h. The light purple color of the solution gradually changes to red and eventually to a pale yellow. The solvent was removed *in vacuo*. Then, 2 mL of diethyl ether was added to the residue, and 10 mL of hexane was added to crash out a pale yellow powder. The powder was washed twice with hexane and then put under reduced pressure to dry. The same procedure can be repeated with **5** to achieve the same results. Yield: 130 mg, 90%. ¹H NMR (400 MHz, CD₂Cl₂): δ 11.90 (br. s, 1H, H7), 9.20 (d, $J_{\text{HH}} = 6$ Hz, 1H, H17), 9.14 (d, $J_{\text{HH}} = 5$ Hz, 1H, H12), 8.37 (t, $J_{\text{HH}} = 8$ Hz, 1H, H15), 8.30 (t, $J_{\text{HH}} = 8$ Hz, 1H, H10), 8.02 (overlaid doublets, 2H, H9 and H14), 7.96 (d, $J_{\text{HH}} = 8$ Hz, 2H, H26), 7.91–7.86 (multiple peaks, 4H, H16, H11, H28, and H22), 7.68 (t, $J_{\text{HH}} = 8$ Hz, 2H, H27), 7.56 (t, $J_{\text{HH}} = 8$ Hz, 1H, H20), 7.49 (t (second-order coupling), 1H, H21), 6.91 (d, $J_{\text{HH}} = 8$ Hz, 1H, H19), 3.52–3.34 (m, 2H, H3 or H6), 3.34–3.19 (m, 2H, H3 or H6), 2.49 (s, 3H, H1), 2.32–2.06 (m, 4H, H4 and H5). Free benzophenone is observed at 7.78 in the ¹H NMR spectrum. ¹³C{¹H} NMR (101 MHz, CD₂Cl₂): δ 216.59 (C24), 162.18 (C18), 157.52 (C17), 152.95 (C12), 151.40 (C13), 149.31 (C8), 148.52 (d, $J_{\text{CF}} = 241$ Hz, *o*-B(C₆F₅)₄), 147.02 (C23), 144.05 (C15), 143.62 (C10), 138.58 (d, $J_{\text{CF}} = 245$ Hz, *p*-B(C₆F₅)₄), 138.46 (C20), 137.88 (C22), 136.71 (d, $J_{\text{CF}} = 248$ Hz, *m*-B(C₆F₅)₄), 136.67 (C28), 133.56 (C21), 133.51 (C25), 133.11 (C19), 131.04 (C26), 130.36 (C16), 129.92 (C27), 129.08 (C11), 126.66 (C14), 126.05 (C9), 72.17 (C2), 52.54 (C3 or C6), 52.47 (C3 or C6), 25.20 (C4 or C5), 25.08 (C4 or C5), 15.20 (C1). ¹⁹F NMR (376 MHz, CD₂Cl₂): δ -133.99 (br. s, $\nu_{1/2} = 40$ Hz, 16F, *o*-C₆F₅), -163.29 (t, $J_{\text{FF}} = 20$ Hz, 8F, *p*-C₆F₅), -167.32 (t, $J_{\text{FF}} = 18$ Hz, 16F, *m*-C₆F₅). Compound **6** was not found to be analytically pure by EA. Deprotonation of **6** followed by recrystallization removes the impurity.**

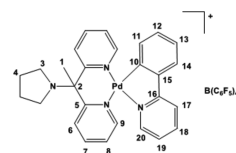


[(Pyr^HCPy₂)Pd(C₆H₄(OCC₆H₅))] ²⁺[BAR^F₄⁻] (7**). Compound **6** (100 mg, 0.082 mmol, 1.0 equiv) was added to a 20 mL scintillation vial with 5 mL of dichloromethane. Potassium carbonate (73 mg, 0.53 mmol, 10 equiv) was added and the mixture was left to stir for 18 h. The solids are removed from the red solution by filtration, and the filtrate was placed under reduced pressure to yield a red powder. **7** can be recrystallized from dichloromethane (~5 mL/100 mg) layered with an equal amount of hexane to give large red crystals after a few days (42 mg, 65%). The leftover solvent can be reduced and relayered with hexane to produce more crystals although the yield will be significantly less than the first. ¹H NMR (400 MHz, CD₂Cl₂): δ 9.01 (d, $J_{\text{HH}} = 5$ Hz, 2H, H9), 8.00 (t, $J_{\text{HH}} = 8$ Hz, 2H, H7), 7.90 (d (second-order coupling), 2H, H17), 7.78–7.71 (multiple peaks, 3H, H19 and H6), 7.69 (d, $J_{\text{HH}} = 8$ Hz, 1H, H13), 7.62 (t (second-order coupling), 2H, H18), 7.50 (ddd, $J_{\text{HH}} = 5$ Hz, 2H, H8), 7.42 (t, $J_{\text{HH}} = 7$ Hz, 1H, H11), 7.28 (t, $J_{\text{HH}} = 8$ Hz, 1H, H12), 6.94 (d, $J_{\text{HH}} = 8$ Hz, 1H, H10), 2.47 (br. s, 4H, H3), 2.11 (s, 3H, H1), 1.64 (br. s, 2H,**

H4), 1.51 (br. s, 2H, H4). ¹³C{¹H} NMR (101 MHz, CD₂Cl₂): δ 213.39 (C16), 164.41 (C10), 160.09 (C5), 153.10 (C9), 145.37 (C15), 140.51 (C7), 136.10 (C12), 135.30 (C17), 135.26 (C14), 134.34 (C20), 133.53 (C11), 130.11 (C18), 129.38 (C19), 125.67 (C8), 125.57 (C13), 123.44 (C6), 68.30 (C2), 46.81 (C3), 23.87 (C4), 11.56 (C1). ¹⁹F NMR (376 MHz, CD₂Cl₂): δ -133.08 (br. s, $\nu_{1/2} = 40$ Hz, 8F, *o*-C₆F₅), -163.72 (t, $J_{\text{FF}} = 20$ Hz, 4F, *p*-C₆F₅), -167.57 (t, $J_{\text{FF}} = 18$ Hz, 8F, *m*-C₆F₅). Before EA, **7** was placed under high vacuum for 72 h and afterward was found to contain 0.3 equiv of dichloromethane by ¹H NMR. Anal. Calcd for C₅₃H₂₈BF₂₀N₃OPd·0.3 CH₂Cl₂: C, 51.40; H, 2.31; N, 3.37. Found: C, 51.05; H, 2.26; N, 3.40.



[(Pyr^HCPy₂)Pd(C₆H₄(NC₅H₄))] ²⁺[BAR^F₄⁻] (8**). Compound **2** (136 mg, 0.285 mmol, 1.0 equiv) was added to a 25 mL Schlenk flask with 10 mL of dichloromethane and 2-phenylpyridine (44 μ L, 0.285 mmol, 1.0 equiv). [H(OEt₂)₂]⁺[BAR^F₄⁻] (255 mg, 0.285 mmol, 1.0 equiv) was slowly added over a minute to the solution with vigorous stirring. After 48 h of stirring, the reaction mixture showed a mixture of products by ¹H NMR. 2-Phenylpyridine (44 μ L, 0.285 mmol, 1.0 equiv) and potassium carbonate (200 mg, 1.45 mmol, 5.1 equiv) was added to the reaction mixture and left to stir for another 48 h. The solids were removed by filtration, and the yellow filtrate was layered with an equivalent volume of hexane in a 20 mL scintillation flask for recrystallization. Large yellow crystals were visible (261 mg, 71%). ¹H NMR (400 MHz, CD₂Cl₂): δ 8.90 (br. s, 2H, H9), 8.03–7.95 (multiple peaks, 4H, H20, H18, and H7), 7.90 (d, $J_{\text{HH}} = 8$ Hz, 1H, H17), 7.71 (d, $J_{\text{HH}} = 8$ Hz, 2H, H6), 7.62 (d, $J_{\text{HH}} = 8$ Hz, 1H, H14), 7.50 (t, $J_{\text{HH}} = 6$ Hz, 2H, H8), 7.23 (multiple peak, 2H, H13 and H12), 7.13 (t, $J_{\text{HH}} = 8$ Hz, 1H, H19), 6.76 (d, $J_{\text{HH}} = 8$ Hz, 1H, H11), 2.56 (br. s, 4H, H3), 2.15 (s, 3H, H1), 1.56 (m, 2H, H4), 1.31 (m, 2H, H4 (overlaid with hexane)). ¹³C{¹H} NMR (101 MHz, CD₂Cl₂): δ 166.27 (C16), 161.04 (C5), 155.76 (C10), 148.67 (C20), 145.54 (C15), 140.45 (C7), 139.86 (C18), 133.44 (C11), 130.53 (C12), 125.70 (C8), 125.53 (C13), 124.31 (C14), 123.38 (C19), 123.22 (C6), 68.53 (C2), 46.84 (C3), 23.80 (C4), 11.28 (C1). ¹⁹F NMR (376 MHz, CD₂Cl₂): δ -133.06 (br. s, $\nu_{1/2} = 40$ Hz, 8F, *o*-C₆F₅), -163.70 (t, $J_{\text{FF}} = 20$ Hz, 4F, *p*-C₆F₅), -167.56 (t, $J_{\text{FF}} = 18$ Hz, 8F, *m*-C₆F₅). Before EA, **8** was placed under high vacuum for 72 h and afterward was found to contain 0.2 equiv of dichloromethane by ¹H NMR. Anal. Calcd for C₅₁H₂₇BF₂₀N₄Pd·0.2 CH₂Cl₂: C, 50.82; H, 2.28; N, 4.63. Found: C, 51.02; H, 2.66; N, 4.41.**



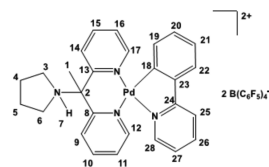
[(Pyr^HCPy₂)Pd(C₆H₄(OCC₆H₅))] ²⁺[SbF₆⁻]₂ (10**). Compound **3** (46 mg, 0.107 mmol, 1.0 equiv), benzophenone (195 mg, 1.07 mmol, 10 equiv) and 10 mL of dichloromethane to a 25 mL Schlenk flask. AgSbF₆ (73.4 mg, 0.214 mmol, 2.0 equiv) was added to the stirred solution and AgCl quickly precipitated. The reaction was left to stir overnight. The AgCl was removed by filtration. The solvent was removed under reduced pressure, and the residue was washed twice with hexane to remove excess benzophenone. The residue was dissolved in ~5 mL of dichloromethane and layered with an equal amount of hexane and left at room temperature overnight. Crystals suitable for X-ray diffraction were available the next day. The ¹H NMR spectrum was consistent with that of the [BAR^F₄⁻] analog.**

[(Pyr^HCPy₂)Pd(C₆H₄(NC₅H₄))] ²⁺[SbF₆⁻]₂ (11**). Compound **3** (49 mg, 0.114 mmol, 1.0 equiv) was added to a 25 mL Schlenk flask with 12 mL of dichloromethane and was stirred vigorously. AgSbF₆ (39 mg, 0.114 mmol, 1.0 equiv) was added to the solution to generate a**

Pd–Cl dimer species (not reported). AgCl precipitate was quickly formed and the solution gained a colloidal purple-black shade. After 15 min, 2-phenylpyridine solution (1.63 mL, 0.07 M in hexanes, 0.114 mmol, 1.0 equiv) was added dropwise, and the solution became dark yellow. After an additional 15 min of stirring, another equivalent of AgSbF₆ (39 mg, 0.114 mmol, 1.0 equiv) was added which produced an initial bright yellow that steadily became brown. The reaction was allowed to stir overnight. The next day AgCl was removed by filtration. The solvent was reduced under reduced pressure to ~5 mL, layered with an equal amount of hexane, and left out at room temperature for 1 day to yield crystals suitable for X-ray diffraction. The ¹H NMR spectrum was consistent with that of the [BAr^F₄][−] analog.

[H(CH₃OH)_{1.5}]⁺[BAr^F₄][−]. [H(OEt)₂]⁺[BAr^F₄][−] (80.0 mg, 0.097 mmol) was added to a 10 mL Schlenk flask with ~2 mL of methanol and was allowed to stir for 1 min before the solvent was removed under reduced pressure. The resulting colorless residue was redissolved in 2 mL of methanol and allowed to stir (~1 min) before the solvent was removed under reduced pressure yielding a colorless residue. This trituration process was repeated once more with methanol, followed by trituration with dichloromethane. The resultant white powder was dissolved in ~1 mL of dichloromethane (in a 3 mL scintillation vial) and layered with ~2 mL of hexane. The vial was sealed and placed in a −32 °C freezer for 24 h, resulting in pale brown crystals (24 mg). [H(CH₃OH)_{1.5}]⁺[BAr^F₄][−] decomposes if left in solution; pentafluorobenzene is one of the primary decomposition products. The reported stoichiometry is based on a best fit to the relative integrals of the OH and CH₃ groups in the ¹H NMR spectrum. Crystals are amenable to X-ray diffraction, but the methanol molecules are disordered and nonresolvable. ¹H NMR (400 MHz, CD₂Cl₂): δ 8.46 (br. s, 2.5 H, CH₃OH₂⁺/CH₃OH), 3.81 (s, 4.5 H, CH₃OH₂⁺/CH₃OH). ¹³C{¹H} NMR (101 MHz, CD₂Cl₂): δ 53.36 (CH₃OH). The methanol carbon peak is directly under the carbon CD₂Cl₂ peak, and its location was determined by ¹H–¹³C HSQC. ¹⁹F NMR (376 MHz, CD₂Cl₂): δ −133.03 (br. s, ν_{1/2} = 40 Hz, 16F, *o*-C₆F₅), −163.29 (t, ³J_{FF} = 20 Hz, 8F, *p*-C₆F₅), −167.35 (t, ³J_{FF} = 18 Hz, 16F, *m*-C₆F₅).

NMR Tube Experiments. *Synthesis of [(pyr^HCPy)₂](C₆H₄(NC₅H₄))] ²⁺[BAr^F₄][−] (9).* Compound 8 (10.2 mg, 0.0085 mmol, 1.0 equiv) and [H(OEt)₂]⁺[BAr^F₄][−] (6.7 mg, 0.0081 mmol, 0.95 equiv) were added to an NMR tube. Then, ~0.5 mL of CD₂Cl₂ was added, and the NMR tube was capped and shaken for 10 s to yield 93% of the expected conversion to the N-protonated dication (based on [Et₂O]). The minor species observed in the NMR spectra is the unprotonated 8. ¹H NMR (400 MHz, CD₂Cl₂): δ 12.86 (br. s, 1H, H7), 9.14 (d, J_{HH} = 6 Hz, 1H, H17), 8.96 (d, J_{HH} = 5 Hz, 1H, H12), 8.30 (multiple peaks, 2H, H15 and H10), 8.14 (t, J_{HH} = 8 Hz, 1H, H26), 8.06–7.95 (multiple peaks, 3H, H9, H25, and H14), 7.93–7.85 (multiple peaks, 3H, H28, H11, and H16), 7.71 (d, J_{HH} = 8 Hz, 1H, H22), 7.40 (t, J_{HH} = 8 Hz, 1H, H21), 7.33 (dd, J_{HH} = 6 Hz, 1H, H27), 7.21 (t, J_{HH} = 8 Hz, 1H, H20), 6.58 (d, J_{HH} = 8 Hz, 1H, H19), 3.48–3.30 (m, 4H, H3 and H6), 2.51 (s, 3H, H1), 2.26 (m, 2H, H4 or H5), 2.06 (m, 2H, H4 or H5). Free diethyl ether is observed at 3.45 and 1.15 in the ¹H NMR spectrum. ¹³C{¹H} NMR (101 MHz, CD₂Cl₂): δ 166.70 (C24), 157.09 (C17), 154.36 (C18), 153.48 (C12), 151.37 (C13), 151.04 (C8), 148.43 (C28), 146.00 (C23), 143.71 (C15), 143.60 (C10), 142.92 (C26), 133.00 (C19), 132.27 (C20), 129.78 (C16), 129.34 (C11), 129.04 (C21), 126.45 (C9), 126.37 (C22), 126.01 (C14), 124.91 (C27), 122.01 (C25), 71.76 (C2), 52.27 (C3 or C6), 52.14 (C3 or C6), 25.09 (C4 and C5), 15.15 (C1). Free diethyl ether is observed at 15.49 and 66.14 in the ¹³C NMR spectrum. ¹⁹F NMR (376 MHz, CD₂Cl₂): δ −133.03 (br. s, ν_{1/2} = 40 Hz, 16F, *o*-C₆F₅), −163.29 (t, ³J_{FF} = 20 Hz, 8F, *p*-C₆F₅), −167.35 (t, ³J_{FF} = 18 Hz, 16F, *m*-C₆F₅).



Protonation Equilibria. Proton Exchange Equilibrium (*p*K_a Determination) of 8 with 2-Methylanilinium in CD₃CN. A J. Young tube was charged with 8 (9.5 mg, 0.008 mmol, 1.0 equiv), 2-methylanilinium [BAr^F₄][−] (14.8 mg, 0.019 mmol, 2.38 equiv), and ~0.5 mL of CD₃CN. The tube was vigorously shaken and ¹H NMR spectra were recorded soon after (<30 min). The initial ¹H NMR spectrum showed a mixture of 8, 9, and the coalesced peaks of 2-methylaniline and 2-methylanilinium B(C₆F₅)₄[−]. ¹H NMR spectra taken of the same sample over the ensuing days show no significant change in the equilibrium concentrations. The experiment was duplicated twice with comparable amounts. The following peaks were used to determine the equilibrium concentration of 8: H9, H20, H14, H11, and H1. The following peaks were used to determine the equilibrium concentration of 9: H7, H12/H17 (appear as one peak), H28, H11/H16 (appear as one peak), and H1. The equilibrium concentration of 2-methylanilinium [BAr^F₄][−] was established by subtracting the normalized equilibrium concentration of 9 from the combined normalized concentration of 2-methylaniline and 2-methylanilinium B(C₆F₅)₄[−]. The equilibrium concentration of 2-methylaniline equals that of 9.

Proton Exchange Equilibrium (*p*K_a Determination) of 8 with 2-Methylanilinium in CD₂Cl₂. A J. Young tube was charged with 8 (9.5 mg, 0.008 mmol, 1.0 equiv), 2-methylanilinium [BAr^F₄][−] (14.8 mg, 0.019 mmol, 2.38 equiv), and ~0.5 mL of CD₂Cl₂. The tube was vigorously shaken, and ¹H NMR spectra were recorded soon after (<30 min). The initial ¹H NMR spectrum showed a mixture of 8 and 9 and the coalesced peaks of 2-methylaniline and 2-methylanilinium B(C₆F₅)₄[−]. ¹H NMR spectra taken of the same sample over the ensuing days show no significant change in the equilibrium concentrations. The experiment was duplicated twice with comparable amounts. The following peaks were used to determine the equilibrium concentration of 8: H9, H8, H14, H11, and H1. The following peaks were used to determine the equilibrium concentration of 9: H7, H17, H12, H19, and H1. The equilibrium concentration of 2-methylanilinium [BAr^F₄][−] was established by subtracting the normalized equilibrium concentration of 9 from the combined normalized concentration of 2-methylaniline and 2-methylanilinium B(C₆F₅)₄[−]. The equilibrium concentration of 2-methylaniline equals that of 9.

Proton Exchange Equilibrium (*p*K_a Determination) of 8 with 2,6-Diisopropylanilinium in CD₃CN. A J. Young tube was charged with 8 (7.8 mg, 0.007 mmol, 1.0 equiv), 2,6-diisopropylanilinium [BAr^F₄][−] (3.0 mg, 0.003 mmol, 0.5 equiv), and ~0.5 mL of CD₃CN. The tube was vigorously shaken and ¹H NMR spectra were recorded soon after (<30 min). The initial ¹H NMR spectrum showed a mixture of 8 and 9 and the coalesced peaks of 2,6-diisopropylaniline and 2,6-diisopropylanilinium B(C₆F₅)₄[−]. ¹H NMR spectra taken of the same sample over the ensuing days show no significant change in the equilibrium concentrations. The experiment was duplicated twice with similar amounts. The following peaks were used to determine the equilibrium concentration of 8: H9, H20, H14, H11, and H1. The following peaks were used to determine the equilibrium concentration of 9: H7, H12/H17 (appear as one peak), H28, H11/H16 (appear as one peak), and H1. The equilibrium concentration of 2,6-diisopropylanilinium [BAr^F₄][−] was established by subtracting the normalized equilibrium concentration of 9 from the combined normalized concentration of 2,6-diisopropylaniline and 2,6-diisopropylanilinium B(C₆F₅)₄[−]. The equilibrium concentration of 2,6-diisopropylaniline equals that of 9.

Proton Exchange Equilibrium (*p*K_a Determination) of 8 with 2,6-Diisopropylanilinium in CD₂Cl₂. A J. Young tube was charged with 8 (4.8 mg, 0.004 mmol, 1.0 equiv), 2,6-diisopropylanilinium [BAr^F₄][−] (4.2 mg, 0.005 mmol, 1.2 equiv), and ~0.5 mL of CD₂Cl₂. The tube was vigorously shaken, and ¹H NMR spectra were recorded soon after

(<30 min). The initial ^1H NMR spectrum showed a mixture of **8** and **9** and the coalesced peaks of 2,6-diisopropylaniline and 2,6-diisopropylanilinium $\text{B}(\text{C}_6\text{F}_5)_4^-$. ^1H NMR spectra taken of the same sample over the ensuing days show no significant change in the equilibrium concentrations. The experiment was duplicated twice with similar amounts. The following peaks were used to determine the equilibrium concentration of **8**: H9, H8, H19, H11, and H1. The following peaks were used to determine the equilibrium concentration of **9**: H7, H17, H12, H19, and H1. The equilibrium concentration of 2,6-diisopropylanilinium $[\text{BAR}^{\text{F}}_4]^-$ was established by subtracting the normalized equilibrium concentration of **9** from the combined normalized concentration of 2,6-diisopropylaniline and 2,6-diisopropylanilinium $\text{B}(\text{C}_6\text{F}_5)_4^-$. The equilibrium concentration of 2,6-diisopropylaniline equals that of **9**.

Proton Exchange Equilibrium (pK_a Determination) of **8 with *N,N*-Dimethylanilinium in CD_3CN .** A J. Young tube was charged with **8** (2.2 mg, 0.002 mmol, 1.0 equiv), *N,N*-dimethylanilinium $[\text{BAR}^{\text{F}}_4]^-$ (3.0 mg, 0.004 mmol, 2.0 equiv), and ~ 0.5 mL of CD_3CN . The tube was vigorously shaken and ^1H NMR spectra were recorded soon after (<30 min). The initial ^1H NMR spectrum showed a mixture of **8** and **9** and the coalesced peaks of *N,N*-dimethylaniline and *N,N*-dimethylanilinium $\text{B}(\text{C}_6\text{F}_5)_4^-$. ^1H NMR spectra taken of the same sample over the ensuing days show no significant change in the equilibrium concentrations. The experiment was duplicated twice with similar amounts. The following peaks were used to determine the equilibrium concentration of **8**: H9, H20, H14, H11, and H1. The following peaks were used to determine the equilibrium concentration of **9**: H7, H12/H17 (appear as one peak), H28, H9/H14 (appear as one peak), and H1. The equilibrium concentration of *N,N*-dimethylanilinium $[\text{BAR}^{\text{F}}_4]^-$ was established by subtracting the normalized equilibrium concentration of **9** from the combined normalized concentration of *N,N*-dimethylaniline and 2 *N,N*-dimethylanilinium $\text{B}(\text{C}_6\text{F}_5)_4^-$. The equilibrium concentration of *N,N*-dimethylaniline equals that of **9**.

Proton Exchange Equilibrium (pK_a Determination) of **6 with **8** in CD_2Cl_2 .** A J. Young tube was charged with **6** (12.5 mg, 0.0066 mmol, 1.0 equiv), **8** (9.9 mg, 0.0083 mmol, 1.3 equiv), and ~ 0.5 mL of CD_2Cl_2 . The tube was vigorously shaken, and ^1H NMR spectra were recorded soon after (<30 min). The initial ^1H NMR spectrum showed a mixture of **6**, **7**, **8**, and **9**. ^1H NMR spectra taken of the same sample over the ensuing days show no significant change in the equilibrium concentrations. The experiment was duplicated twice with similar amounts. The following peaks were used to determine the equilibrium concentration of **6**: H7, H17, H12, H19, and H1. The following peaks were used to determine the equilibrium concentration of **7**: H9, H10, and H1. The following peaks were used to determine the equilibrium concentration of **8**: H9, H11, and H1. The following peaks were used to determine the equilibrium concentration of **9**: H7, H17, H12, H19, and H1.

Proton Exchange Equilibrium of **6 with MeOH in CD_2Cl_2 .** A J. Young tube was charged with $[\text{H}(\text{MeOH})_{1.5}]^+[\text{BAR}^{\text{F}}_4]^-$ (7.4 mg, 0.010 mmol equiv) and **7** (5.8 mg, 0.005 mmol) with ~ 0.5 mL of CD_2Cl_2 . The tube was sealed, shaken, and the initial ^1H NMR showed that all of **7** had converted to its protonated analog **6**. A small drop of MeOH was added, and the solution gained a faint red color (^1H NMR revealed a mixture of **6** and **7**, in a 7:1 ratio). After adding ~ 30 equiv of methanol (~ 30 mM), the solution turned completely red, and the ^1H NMR spectrum shows only **7**.

Benzophenone- d_{10} Exchange with **6 in CD_2Cl_2 .** Compound **6** (6.3 mg, 0.006 mmol, 1 equiv) was added to a J. Young tube with benzophenone- d_{10} (0.25 mL, 264 mM in CD_2Cl_2 , 20 equiv). An additional 0.25 mL of CD_2Cl_2 was added, and the tube was sealed and shaken. An initial ^1H NMR spectrum was taken before the sample was heated to 60°C in an oil bath. ^1H NMR spectra of the reaction were collected over the ensuing 2 weeks.

Addition of 2-Phenylpyridine to **4.** Compound **4** (19.6 mg, 0.009 mmol, 1 equiv) was added to a J. Young tube with 2-phenylpyridine (88 μ , 0.006 mmol, 0.66 equiv) and 0.5 mL of CD_2Cl_2 . After 3 days, the reaction mixture contains compounds **4**, **8**, and **9** in a ratio of 0.50:0.12:1.00 (by ^1H NMR). An additional amount of 2-phenyl-

pyridine (34 μ , 0.003 mmol, 0.34 equiv) was added to the NMR tube, and the reaction was left to sit. After 8 days, the reaction mixture contains compounds **4**, **8**, and **9** in a ratio of 0.08:0.11:1.00 (by ^1H NMR). 2-phenylpyridine was added stepwise to decrease the formation of 2-phenylpyridinium which once formed significantly reduces the rate of cyclometalation

■ ASSOCIATED CONTENT

📄 Supporting Information

The Supporting Information is available free of charge on the ACS Publications website at DOI: 10.1021/acs.organomet.8b00348.

Experimental procedures, syntheses, computational details, and X-ray crystallographic data (PDF)

Cartesian coordinates (XYZ)

Accession Codes

CCDC 1840201–1840206 contain the supplementary crystallographic data for this paper. These data can be obtained free of charge via www.ccdc.cam.ac.uk/data_request/cif, or by emailing data_request@ccdc.cam.ac.uk, or by contacting The Cambridge Crystallographic Data Centre, 12 Union Road, Cambridge CB2 1EZ, UK; fax: +44 1223 336033.

■ AUTHOR INFORMATION

Corresponding Author

*E-mail: ehulley@uwyo.edu.

ORCID

William E. Christman: 0000-0002-5716-6859

Navamoney Arulsamy: 0000-0001-5274-0906

Elliott B. Hulley: 0000-0002-2630-3689

Notes

The authors declare no competing financial interest.

■ ACKNOWLEDGMENTS

We gratefully acknowledge financial support from the UW Office of Vice President of Research, UW School of Energy Resources, and the UW Department of Chemistry. We gratefully acknowledge financial support from the National Science Foundation (CHE 0619920) for the purchase of the Bruker Apex II Diffractometer and National Institute of General Medical Sciences of the National Institutes of Health (from the Institutional Development Award, Grant no. 2P20GM103432) for the purchase of the Oxford Cobra Cryo system. DFT calculations were performed on an allocation at the Advanced Research Computing Center at the University of Wyoming ("Mt. Moran", <http://n2t.net/ark:/85786/m4159c>). We are also indebted to Prof. Robert Corcoran and Prof. Dean Roddick for helpful discussions.

■ REFERENCES

- (1) Shilov, A. E.; Shul'pin, G. B. Activation of C–H Bonds by Metal Complexes. *Chem. Rev.* **1997**, *97* (8), 2879–2932.
- (2) Lyons, T. W.; Sanford, M. S. Palladium-Catalyzed Ligand-Directed C–H Functionalization Reactions. *Chem. Rev.* **2010**, *110* (2), 1147–1169.
- (3) He, J.; Wasa, M.; Chan, K. S. L.; Shao, Q.; Yu, J. Q. Palladium-Catalyzed Transformations of Alkyl C–H Bonds. *Chem. Rev.* **2017**, *117* (13), 8754–8786.
- (4) Labinger, J. A. Platinum-Catalyzed C–H Functionalization. *Chem. Rev.* **2017**, *117* (13), 8483–8496.
- (5) Newton, C. G.; Wang, S. G.; Oliveira, C. C.; Cramer, N. Catalytic Enantioselective Transformations Involving C–H Bond

Cleavage by Transition-Metal Complexes. *Chem. Rev.* **2017**, *117* (13), 8908–8976.

(6) Xue, X. S.; Ji, P.; Zhou, B.; Cheng, J. P. The Essential Role of Bond Energetics in C–H Activation/Functionalization. *Chem. Rev.* **2017**, *117* (13), 8622–8648.

(7) Kubas, G. J. Fundamentals of H₂ Binding and Reactivity on Transition Metals Underlying Hydrogenase Function and H₂ Production and Storage. *Chem. Rev.* **2007**, *107* (10), 4152–4205.

(8) Crabtree, R. H. Dihydrogen Complexation. *Chem. Rev.* **2016**, *116* (15), 8750–8769.

(9) Cope, A. C.; Friedrich, E. C. Electrophilic Aromatic Substitution Reactions by Platinum (II) and Palladium (II) Chlorides on *N,N*-Dimethylbenzylamines. *J. Am. Chem. Soc.* **1968**, *90* (4), 909–913.

(10) Stock, L. M.; Tse, K.; Vorvick, L. J.; Walstrum, S. A. Palladium(II) Acetate Catalyzed Aromatic Substitution Reaction. *J. Org. Chem.* **1981**, *46* (8), 1757–1759.

(11) Lafrance, M.; Rowley, C. N.; Woo, T. K.; Fagnou, K. Catalytic Intermolecular Direct Arylation of Perfluorobenzenes. *J. Am. Chem. Soc.* **2006**, *128* (27), 8754–8756.

(12) Gorelsky, S. I.; Lapointe, D.; Fagnou, K. Analysis of the Concerted Metalation-Deprotonation Mechanism in Palladium-Catalyzed Direct Arylation Across a Broad Range of Aromatic Substrates. *J. Am. Chem. Soc.* **2008**, *130* (33), 10848–10849.

(13) Cook, A. K.; Sanford, M. S. Mechanism of the Palladium-Catalyzed Arene C–H Acetoxylation: A Comparison of Catalysts and Ligand Effects. *J. Am. Chem. Soc.* **2015**, *137* (8), 3109–3118.

(14) Neufeldt, S. R.; Sanford, M. S. Controlling Site Selectivity in Palladium-Catalyzed C–H Bond Functionalization. *Acc. Chem. Res.* **2012**, *45* (6), 936–946.

(15) Catellani, M.; Mealli, C.; Motti, E.; Paoli, P.; Perez-Carreño, E.; Pregosin, P. S. Palladium-Arene Interactions in Catalytic Intermediates: An Experimental and Theoretical Investigation of the Soft Rearrangement between η^1 and η^2 Coordination Modes. *J. Am. Chem. Soc.* **2002**, *124* (16), 4336–4346.

(16) Yamamoto, K.; Kimura, S.; Murahashi, T. σ - π Continuum in Indole-Palladium(II) Complexes. *Angew. Chem., Int. Ed.* **2016**, *55* (17), 5322–5326.

(17) Koper, M. T. M.; Bouwman, E. Electrochemical Hydrogen Production: Bridging Homogeneous and Heterogeneous Catalysis. *Angew. Chem., Int. Ed.* **2010**, *49* (22), 3723–3725.

(18) Smalley, A. P.; Gaunt, M. J. Mechanistic Insights into the Palladium-Catalyzed Aziridination of Aliphatic Amines by C–H Activation. *J. Am. Chem. Soc.* **2015**, *137* (33), 10632–10641.

(19) Morrow, T. J.; Christman, W. E.; Williams, J. Z.; Arulsamy, N.; Goroncy, A.; Hulley, E. B. Ligand Dynamics and Protonation Preferences of Rh and Ir Complexes Bearing an Almost, but Not Quite, Pendent Base. *Dalt. Trans.* **2018**, *47* (8), 2670–2682.

(20) Augustin-Nowacka, D.; Chmurzyński, L. A Potentiometric Study of Acid-Base Equilibria of Substituted Pyridines in Acetonitrile. *Anal. Chim. Acta* **1999**, *381* (2–3), 215–220.

(21) Espinosa, S.; Bosch, E.; Rosés, M. Retention of Ionizable Compounds in High-Performance Liquid Chromatography 14. Acid-Base PK Values in Acetonitrile-Water Mobile Phases. *J. Chromatogr. A* **2002**, *964* (1–2), 55–66.

(22) Leffek, K. T.; Pruszyński, P.; Thanapaalasingham, K. Basicity of Substituted 2-Phenyl-1,1,3,3-Tetramethylguanidines and Other Bases in Acetonitrile Solvent. *Can. J. Chem.* **1989**, *67* (4), 590–595.

(23) Morris, R. H. Brønsted–Lowry Acid Strength of Metal Hydride and Dihydrogen Complexes. *Chem. Rev.* **2016**, *116* (15), 8588–8654.

(24) Hunter, K. N. H. C. A.; Lehn, M. J. K. J.; Olivucci, S. V. L. M.; Venturi, J. T. M.; Yamamoto, C. W. H. W. H. C–H Activation; Yu, J.-Q.; Shi, Z., Eds.; Topics in Current Chemistry; Springer Berlin Heidelberg: Berlin, Heidelberg, 2010; Vol. 292.

(25) Li, C.; Cheng, C.; Liao, F.-L.; Wang, S. Insertion of Norbornadiene into the Aryl–Palladium Bond; Synthesis, Structure and Dynamics of Intramolecular η^2 -Arene Palladium Species. *J. Chem. Soc., Chem. Commun.* **1991**, 710–712.

(26) Yin, J.; Rainka, M. P.; Zhang, X.-X.; Buchwald, S. L. A Highly Active Suzuki Catalyst for the Synthesis of Sterically Hindered Biaryls:

Novel Ligand Coordination. *J. Am. Chem. Soc.* **2002**, *124* (7), 1162–1163.

(27) Walker, S. D.; Barder, T. E.; Martinelli, J. R.; Buchwald, S. L. A Rationally Designed Universal Catalyst for Suzuki–Miyaura Coupling Processes. *Angew. Chem., Int. Ed.* **2004**, *43* (14), 1871–1876.

(28) Christmann, U.; Vilar, R.; White, A. J. P.; Williams, D. J. Synthesis of Two Novel Dinuclear Palladium(I) Complexes and Studies of Their Catalytic Activity in Amination Reactions. *Chem. Commun.* **2004**, 2 (11), 1294–1295.

(29) Connelly, S. J.; Chanez, A. G.; Kaminsky, W.; Heinekey, D. M. Characterization of a Palladium Dihydrogen Complex. *Angew. Chem., Int. Ed.* **2015**, *54* (20), 5915–5918.

(30) Vigalok, A.; Uzan, O.; Shimon, L. J. W.; Ben-David, Y.; Martin, J. M. L.; Milstein, D. Formation of η^2 C–H Agostic Rhodium Arene Complexes and Their Relevance to Electrophilic Bond Activation. *J. Am. Chem. Soc.* **1998**, *120* (48), 12539–12544.

(31) Zhao, Y.; Truhlar, D. G. The M06 Suite of Density Functionals for Main Group Thermochemistry, Thermochemical Kinetics, Noncovalent Interactions, Excited States, and Transition Elements: Two New Functionals and Systematic Testing of Four M06-Class Functionals and 12 Other Function. *Theor. Chem. Acc.* **2008**, *120* (1–3), 215–241.

(32) Weigend, F. Accurate Coulomb-Fitting Basis Sets for H to Rn. *Phys. Chem. Chem. Phys.* **2006**, *8* (9), 1057.

(33) Marenich, A. V.; Cramer, C. J.; Truhlar, D. G. Universal Solvation Model Based on Solute Electron Density and on a Continuum Model of the Solvent Defined by the Bulk Dielectric Constant and Atomic Surface Tensions. *J. Phys. Chem. B* **2009**, *113* (18), 6378–6396.

(34) Kaljurand, I.; Kütt, A.; Sooväli, L.; Rodima, T.; Mäemets, V.; Leito, I.; Koppel, I. A. Extension of the Self-Consistent Spectrophotometric Basicity Scale in Acetonitrile to a Full Span of 28 p K a Units: Unification of Different Basicity Scales. *J. Org. Chem.* **2005**, *70* (3), 1019–1028.

(35) Kaupmees, K.; Järviste, R.; Leito, I. Basicity of Very Weak Bases in 1,2-Dichloroethane. *Chem. - Eur. J.* **2016**, *22* (48), 17445–17449.

(36) Kolthoff, I. M.; Chantooni, M. K. Protonation in Acetonitrile of Water, Alcohols, and Diethyl Ether. *J. Am. Chem. Soc.* **1968**, *90* (13), 3320–3326.

(37) Kolthoff, I. M.; Bruckenstein, S.; Chantooni, M. K. Acid-Base Equilibria in Acetonitrile. Spectrophotometric and Conductometric Determination of the Dissociation of Various Acids. *J. Am. Chem. Soc.* **1961**, *83* (19), 3927–3935.

(38) Fujinaga, T.; Sakamoto, I. Electrochemical Studies of Sulfonates in Non-Aqueous Solvents. *J. Electroanal. Chem. Interfacial Electrochem.* **1977**, *85* (1), 185–201.

(39) Haav, K.; Saame, J.; Kütt, A.; Leito, I. Basicity of Phosphanes and Diphosphanes in Acetonitrile. *Eur. J. Org. Chem.* **2012**, *2012* (11), 2167–2172.

(40) Kolthoff, I. M.; Chantooni, M. K. Effect of Molecular Acid-Base Dissociation of Salts on Conductometric Titration Curves in Acetonitrile. *J. Am. Chem. Soc.* **1965**, *87* (5), 1004–1012.

(41) Room, E. I.; Kaljurand, I.; Leito, I.; Rodima, T.; Koppel, I. A.; Vlasov, V. M. Acid-Base Equilibria in Nonpolar Media. 3. Expanding the Spectrophotometric Acidity Scale in Heptane. *J. Org. Chem.* **2003**, *68* (20), 7795–7799.

(42) Daasbjerg, K.; Oslob, J. D.; Åkermark, B.; Norrby, P.-O. Estimation of the PKa for Some Hydrocarbons and Aldehydes and Solvation Energies of the Corresponding Anions. *Acta Chem. Scand.* **1995**, *49*, 878–887.

(43) Fu, Y.; Liu, L.; Li, R.-Q.; Liu, R.; Guo, Q.-X. First-Principle Predictions of Absolute p K a 's of Organic Acids in Dimethyl Sulfoxide Solution. *J. Am. Chem. Soc.* **2004**, *126* (3), 814–822.

(44) Fu, Y.; Liu, L.; Yu, H. Z.; Wang, Y. M.; Guo, Q. X. Quantum-Chemical Predictions of Absolute Standard Redox Potentials of Diverse Organic Molecules and Free Radicals in Acetonitrile. *J. Am. Chem. Soc.* **2005**, *127* (19), 7227–7234.

(45) Luo, Y.-R. *Comprehensive Handbook of Chemical Bond Energies*; CRC Press: Boca Raton, FL, 2007.

- (46) Kubas, G. J. Activation of Dihydrogen and Coordination of Molecular H₂ on Transition Metals. *J. Organomet. Chem.* **2014**, *751*, 33–49.
- (47) Cheng, G. J.; Yang, Y. F.; Liu, P.; Chen, P.; Sun, T. Y.; Li, G.; Zhang, X.; Houk, K. N.; Yu, J. Q.; Wu, Y. D. Role of N-Acyl Amino Acid Ligands in Pd(II)-Catalyzed Remote C-H Activation of Tethered Arenes. *J. Am. Chem. Soc.* **2014**, *136* (3), 894–897.
- (48) Ke, Z.; Cundari, T. R. Palladium-Catalyzed C-H Activation/C-N Bond Formation Reactions: DFT Study of Reaction Mechanisms and Reactive Intermediates. *Organometallics* **2010**, *29* (4), 821–834.
- (49) Siegbahn, P. E. M.; Crabtree, R. H. Modeling the Solvent Sphere: Mechanism of the Shilov Reaction. *J. Am. Chem. Soc.* **1996**, *118* (18), 4442–4450.
- (50) Rakowski DuBois, M.; DuBois, D. L. Development of Molecular Electrocatalysts for CO₂ Reduction and H₂ Production/Oxidation. *Acc. Chem. Res.* **2009**, *42* (12), 1974–1982.
- (51) Goldsmith, B. R.; Hwang, T.; Seritan, S.; Peters, B.; Scott, S. L. Rate-Enhancing Roles of Water Molecules in Methyltrioxorhenium-Catalyzed Olefin Epoxidation by Hydrogen Peroxide. *J. Am. Chem. Soc.* **2015**, *137* (30), 9604–9616.
- (52) Matheu, R.; Ertem, M. Z.; Benet-Buchholz, J.; Coronado, E.; Batista, V. S.; Sala, X.; Llobet, A. Intramolecular Proton Transfer Boosts Water Oxidation Catalyzed by a Ru Complex. *J. Am. Chem. Soc.* **2015**, *137* (33), 10786–10795.
- (53) Kickham, J. E.; Loeb, S. J. Unusual Interaction of Ag⁺ with an Organopalladium Crown Ether. Synthesis and Structures of [PdCl(L)] and [Pd(H₂O)(L)(Ag)][CF₃SO₃]₂ (L = 5,8,11-Trioxa-2,14-Dithia-[15]-m-Cyclophane). *Organometallics* **1995**, *14* (7), 3584–3587.
- (54) Lotz, M. D.; Camasso, N. M.; Canty, A. J.; Sanford, M. S. Role of Silver Salts in Palladium-Catalyzed Arene and Heteroarene C–H Functionalization Reactions. *Organometallics* **2017**, *36* (1), 165–171.
- (55) Khusnutdinova, J. R.; Rath, N. P.; Mirica, L. M. The Conformational Flexibility of the Tetradentate Ligand ^tBuN₄ Is Essential for the Stabilization of (^tBuN₄)Pd^{III} Complexes. *Inorg. Chem.* **2014**, *53* (24), 13112–13129.
- (56) Jutzi, P.; Mueller, C.; Stammer, A.; Stammer, H.-G. Synthesis, Crystal Structure, and Application of the Oxonium Acid [H-(OEt₂)₂]⁺[B(C₆F₅)₄]⁻. *Organometallics* **2000**, *19* (7), 1442–1444.
- (57) Fulmer, G. R.; Miller, A. J. M.; Sherden, N. H.; Gottlieb, H. E.; Nudelman, A.; Stoltz, B. M.; Bercau, J. E.; Goldberg, K. I. NMR Chemical Shifts of Trace Impurities: Common Laboratory Solvents, Organics, and Gases in Deuterated Solvents Relevant to the Organometallic Chemist. *Organometallics* **2010**, *29* (9), 2176–2179.
- (58) Frisch, M. J.; Trucks, G. W.; Schlegel, H. B.; Scuseria, G. E.; Robb, M. A.; Cheeseman, J. R.; Scalmani, G.; Barone, V.; Mennucci, B.; Petersson, G. A.; et al. Gaussian09 Revision D.01. *Gaussian 09 Revision D.01*. Gaussian Inc.: Wallingford CT, 2010.
- (59) Zhao, Y.; Truhlar, D. G. A New Local Density Functional for Main-Group Thermochemistry, Transition Metal Bonding, Thermochemical Kinetics, and Noncovalent Interactions. *J. Chem. Phys.* **2006**, *125*, 194101.
- (60) Chai, J.-D.; Head-Gordon, M. Long-Range Corrected Hybrid Density Functionals with Damped Atom–Atom Dispersion Corrections. *Phys. Chem. Chem. Phys.* **2008**, *10* (44), 6615.
- (61) Becke, A. D. Density-Functional Thermochemistry. III. The Role of Exact Exchange. *J. Chem. Phys.* **1993**, *98* (7), 5648–5652.
- (62) Weigend, F.; Ahlrichs, R. Balanced Basis Sets of Split Valence, Triple Zeta Valence and Quadruple Zeta Valence Quality for H to Rn: Design and Assessment of Accuracy. *Phys. Chem. Chem. Phys.* **2005**, *7* (18), 3297.
- (63) Mennucci, B.; Tomasi, J.; Cammi, R.; Cheeseman, J. R.; Frisch, M. J.; Devlin, F. J.; Gabriel, S.; Stephens, P. J. Polarizable Continuum Model (PCM) Calculations of Solvent Effects on Optical Rotations of Chiral Molecules. *J. Phys. Chem. A* **2002**, *106* (25), 6102–6113.
- (64) Carole, W. A.; Colacot, T. J. Understanding Palladium Acetate from a User Perspective. *Chem. - Eur. J.* **2016**, *22* (23), 7649